

Quantum critical point with infinite projected entangled paired states

Didier Poilblanc and Matthieu Mambrini¹

¹*Laboratoire de Physique Théorique, C.N.R.S. and Université de Toulouse, 31062 Toulouse, France*
(Dated: May 15, 2022)

A classification of SU(2)-invariant Projected Entangled Paired States (PEPS) on the square lattice, based on a unique site tensor, has been recently introduced by Mambrini et al. [1]. It is not clear whether such SU(2)-invariant PEPS can either i) exhibit long-range magnetic order (like in the Néel phase) or ii) describe a genuine Quantum Critical Point (QCP) separating two ordered phases. Here, we identify a specific family of SU(2)-invariant PEPS of the classification which provides excellent variational energies for the $J_1 - J_2$ frustrated Heisenberg model, especially at $J_2 = 0.5$, corresponding to the approximate location of the QCP separating the Néel phase from a Quantum Disordered phase. The PEPS are build from virtual states belonging to the $\frac{1}{2}^{\otimes N} \oplus 0$ SU(2)-representation, i.e. with N “colors” of virtual spin- $\frac{1}{2}$. Using a full update infinite-PEPS approach directly in the thermodynamic limit, based on the Corner Transfer Matrix renormalization algorithm supplemented by a Conjugate Gradient optimization scheme, we provide evidence of i) the absence of magnetic order and ii) critical behaviors both in the singlet and triplet channels (when the number of colors $N \geq 3$). We argue that such a PEPS gives a qualitative description of the critical point of the $J_1 - J_2$ model.

PACS numbers: 75.10.Kt, 75.10.Jm

I. INTRODUCTION

Low-dimensional quantum magnets offer a rich zoo of phases breaking a discrete (like point group or lattice) or a continuous (like spin rotation) symmetry. Often, such phases are separated by Quantum Critical Points (QCP), as described within the usual Ginsburg-Landau (GL) framework. Interestingly, it has been proposed that some QCP may *not* be described by the GL paradigm [2, 3]. A celebrated quantum spin model is the frustrated spin- $\frac{1}{2}$ Heisenberg model on the two-dimensional (2D) square lattice involving competition between nearest neighbor (NN) and next-nearest neighbor (NNN) antiferromagnetic (AF) couplings, J_1 and J_2 respectively. Setting $J_1 = 1$, J_2 controls the amount of frustration which is maximum (classically) at $J_2 = 0.5$. Large-scale Quantum Monte Carlo (QMC) simulations [4–6] has shown that the GS of the unfrustrated ($J_2 = 0$) Heisenberg model exhibits long range (LR) AF order. In the thermodynamic limit, the (global) spin-rotational SU(2) symmetry is spontaneously broken and the GS acquires a finite local staggered magnetization. When J_2 is turned on, the order parameter is gradually suppressed and a quantum phase transition to a Quantum Disordered (QD) phase [7–10] – such as a dimer [11–14] or a plaquette [15, 16] Valence Bond Crystal (VBC) – takes place (see Fig. 1). It was also argued that magnetic frustration could stabilize spin liquids (with no symmetry breaking), such as the Resonating Valence Bond (RVB) states [17] showing algebraic (short range) VBC correlations on the square (Kagome) lattice [18–20].

Recently, tremendous progress have been made in tensor network techniques [21–25], aiming to go beyond Density Matrix Renormalization Group (DMRG) methods [26] in 2D. More specifically, Projected Entangled Pair States (PEPS) [27] are variational ansätze con-

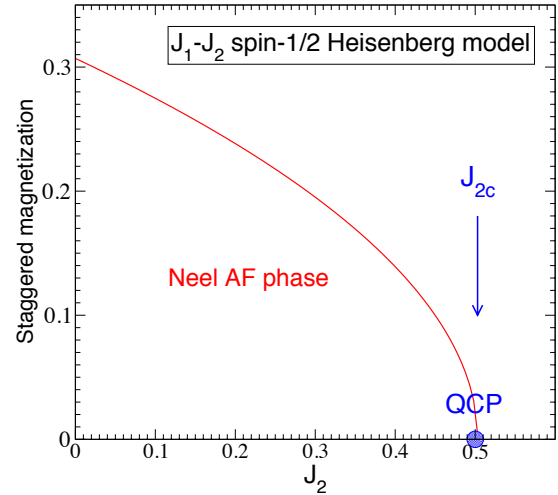


FIG. 1. [Color online] Schematic behavior of the staggered magnetization of the spin- $\frac{1}{2}$ $J_1 - J_2$ Heisenberg model (J_1 is set to 1). m_{stag} vanishes at the QCP. The exact location J_{2c} of the QCP, although still debated, may be close to 0.5.

structed from a few local tensors, located on M non-equivalent sites, and characterized by (i) one bond carrying the physical degrees of freedom (of dimension 2 for spin- $\frac{1}{2}$ systems) and (ii) z “virtual” bonds (z is the lattice coordination number, $z = 4$ for the square lattice) of arbitrary dimension D as shown in Fig. 2(a). Interestingly, any local (gauge) or global (physical) symmetry can be implemented in PEPS [1, 28–35]. Also, a simple bulk-edge (holographic) correspondence provides a remarkable tool to investigate the properties of edge states [36, 37]. Many remarkable states of matter such as trivial paramagnets [38], topological [19, 20, 39] or al-

gebraic [19] RVB spin liquids, loop spin liquids [40], superfluids [41] or unconventional correlated superconductors [42] have simple representations in terms of PEPS. Numerical calculations with PEPS do not require to compute the wave function coefficients (which, conceptually, are given by contracting the tensor network over all virtual links) but, rather, make use of transfer matrices [43] based on “double-layer” tensors (see Fig. 2(b-e)). In the infinite-PEPS (iPEPS) method [44], one works directly in the thermodynamic limit by approximating the (infinite) space around a small M -site cluster by an effective “environment” (see Fig. 2(f)). One of the most accurate computation of the environment is based on a Tensor Renormalization Group (TRG) scheme involving Corner Transfer Matrices (CTM) [45–47] as shown in Fig. 2(g,h). Unrestricted energy minimization over the MdD^z tensor coefficients can be performed using Time Evolution Block Decimation (TEBD) [48, 49] which has to be combined with a simple update [50, 51] or a full update [52] of the environment. A (finite) PEPS method using a 2×2 cluster update supplemented by a finite size extrapolation has also been introduced [53]. Recently, a new optimization scheme using a Conjugate Gradient (CG) algorithm has been tested on the non-frustrated [54, 55] and frustrated [56] Heisenberg model, with iPEPS or finite PEPS, respectively.

The entanglement entropy (i.e. the quantity measuring the amount of entanglement in a bi-partitioned system) in a spontaneously-broken state exhibits anomalous additive logarithmic corrections [57–59] to the area law (i.e. the linear scaling of the entropy with the length of the cut). When the staggered magnetization $m_{\text{stag}} \rightarrow 0$, at the QCP, the violation of the area law is expected to be even more severe. This means that a good description of the QCP, or even of the Néel state, in terms of a PEPS (which strictly fulfills the area law for any finite D) is particularly challenging. A very simple ($D = 3$) PEPS ansatz for the Néel state on the square lattice was first proposed in terms of a (one-parameter) spinon-doped RVB phase [60]. Also, finite size PEPS [61] or, more recently, state-of-the-art iPEPS calculations involving a Conjugate Gradient (CG) minimization algorithm [54, 55] came up with very accurate energy for the Néel GS of the 2D Heisenberg model. However, the phase diagram of the $J_1 - J_2$ model is still heavily debated. No agreement has been reached between several numerical approaches, neither on the nature of the QD region – with proposals of VBC [14, 16, 62, 63], (topological) gapped [64] or gapless [63, 65–67] spin liquids – nor on the location $J_2 = J_{2c}$ of the phase transition. While early Exact Diagonalisations (ED) extrapolations [14] were bracketing $J_{2c} \in [0.34, 0.6]$, DMRG studies [63, 64] suggested $J_{2c} \simeq 0.41 - 0.44$, while Variational Monte Carlo (VMC) studies [67] give $J_{2c} \simeq 0.48(2)$ and finite-size (cluster update) PEPS computations [53] $J_{2c} \simeq 0.572(5)$. Recently, Wang and Sandvik [68] used DMRG to show that the critical point is larger than 0.5. In all these approaches (except ED), the spin rotational

SU(2) symmetry is *explicitly* broken in the Néel phase. However, there is no obstruction principle to construct accurate SU(2)-symmetric wave functions exhibiting long range AF order [69]. Since such states may be characterized by a large entanglement, it is unclear whether it can be realized with low- D symmetric PEPS. Also, whether SU(2)-symmetric PEPS have the potential to describe zero-temperature QCP – in the same way as one-dimensional (1D) Matrix Product States (MPS) can describe critical 1D systems [70–72] – is still unclear [73]. Though, it is known that non-trivial criticality can be captured by PEPS, even at finite D [74].

Motivated by the above conceptual and practical issues, we have re-visited the $J_1 - J_2$ model using some new PEPS developments, based on a general scheme to construct SU(2)-symmetric PEPS using computer-assisted algebra [1]. This enables us to introduce novel key features in the full-update iPEPS scheme : (i) Full translational and rotational invariance is enforced by using a unique SU(2)-invariant tensor on every lattice site; (ii) Full optimization of the (few) tensor coefficients is accomplished via a CG method; (iii) Careful scaling with environment dimension χ is performed in order to address the $\chi \rightarrow \infty$ limit. Using this procedure, we have identified a specific (low-dimensional) family of SU(2)-symmetric PEPS which provides excellent variational energies for the $J_1 - J_2$ frustrated Heisenberg model, especially at $J_2 = 0.5$, i.e. close to the (unknown) QCP of this model. We show evidence that these (optimized) PEPS do not exhibit long range AF order. We also find that, above bond dimension $D = 7$, the PEPS (optimized for $J_2 = 0.5$) exhibits algebraic spin-spin and dimer-dimer correlations (and a small m_{stag} induced by the iPEPS environment vanishes in the limit of infinite environment dimension). Hence, we propose that this state offers a realization of the QCP.

II. SYMMETRIC PEPS ANSÄTZE

We wish here to consider transitionally invariant fully symmetric PEPS in order to (i) reduce the number of independent variational parameters and (ii) provide a good description of the critical point where both SU(2) and lattice symmetries are preserved. For this purpose, we shall use the elegant classification of SU(2)-invariant PEPS tensors on the square lattice [1] according to (i) their virtual degrees of freedom and (ii) how they transform w.r.t the (lattice) point group symmetries (see Fig. 2(a)). For simplicity, we shall a priori restrict ourselves to tensors fully invariant under all operations of the C_{4v} point group (i.e. belonging to the so-called A_1 IRREP). The tensors are further classified according to their virtual space V given by a direct sum of SU(2) IRREPs or “spins”, i.e. $V = \bigoplus_{\alpha} s_{\alpha}$. Restricting to bond dimension $D \leq 7$, the classes of interest here are defined by $V = \frac{1}{2} \oplus 0$ ($D = 3$), $V = \frac{1}{2} \oplus 0 \oplus 0$ ($D = 4$), $V = 1 \oplus \frac{1}{2}$ ($D = 5$), $V = \frac{1}{2} \oplus \frac{1}{2} \oplus 0$ ($D = 5$), $V = \frac{1}{2} \oplus \frac{1}{2} \oplus \frac{1}{2} \oplus 0$ ($D = 7$),

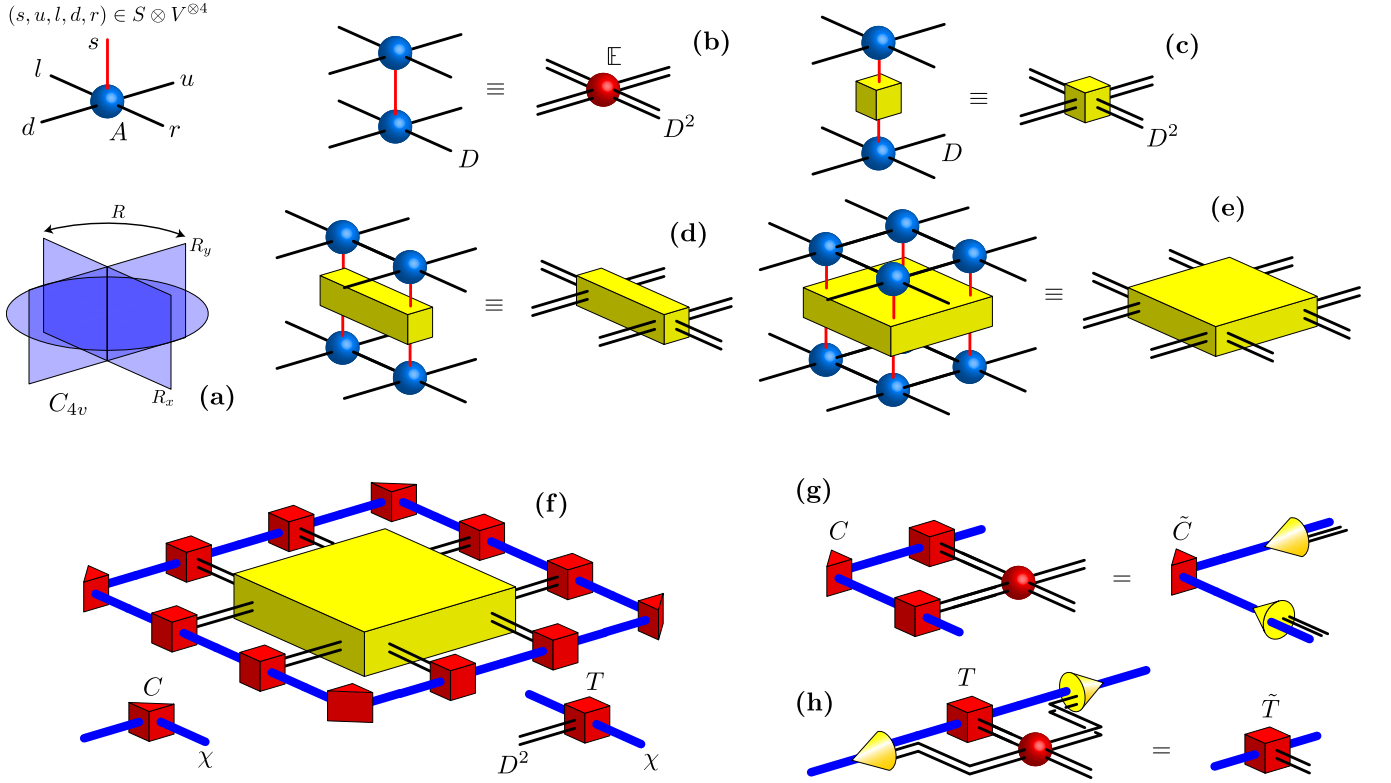


FIG. 2. [Color online] (a) Symmetric PEPS tensor A with one physical index $s = \pm \frac{1}{2}$ and four virtual indices u, l, d and r (of dimension D). A is invariant under the generators of the C_{4v} point group, i.e. the 90-degree rotation R , the reflection R_x and the inversion $I = R_x R_y$. (b-e) The “two layer” (TL) tensors have bond dimension D^2 (double lines). One-site, two-site and four-site TL tensors obtained by inserting the identity \mathbb{I} , a one-site, a two-site and a four-site operator, respectively. (f) iPEPS CTM method : a 2×2 cluster is surrounded by a (self-consistent) environment build from a corner $\chi \times \chi$ transfer matrix C and a side $\chi \times D^2 \times \chi$ tensor T . In practice, we choose $\chi = kD^2$, $k \in \mathbb{N}$. Here the operator inserted on the 4-site is either $\mathbb{I}^{\otimes 4}$ (normalization) or the $J_1 - J_2$ Hamiltonian. (g) Tensor renormalisation scheme : after one site is added, the new $\chi D^2 \times \chi D^2$ CTM is diagonalized and only the largest (in modulus) χ eigenvalues are kept to get the new CTM. (h) The unitaries approximated by isometries (yellow pyramids) are used to compute the new edge tensor.

spanned by a small number \mathcal{D} of independent tensors, $\mathcal{D} = 2, 8, 4, 10, 30$ respectively, given in the Supplementary Materials of Ref. 1 (except for $D = 7$ given in the Supplementary Materials of this paper [75]). Note that a π -rotation of the spin basis is assumed on the sites of one of the two sublattices of the square lattice. In this basis, a genuine $\mathbf{q} = \mathbf{q}_{\text{AF}} \equiv (\pi, \pi)$ (spontaneous) magnetic order translates into a *uniform* $\mathbf{q} = 0$ (spontaneous) magnetization.

The iPEPS method combined with full tensor optimization – We shall now focus on the $J_1 - J_2$ spin- $\frac{1}{2}$ Heisenberg model with NN and NNN antiferromagnetic coupling J_1 and J_2 , respectively, which we have studied at $J_2 = 0$ in the absence of frustration and, for strong frustration, at $J_2 = 0.5$ and $J_2 = 0.55$. Our first goal is to optimize the variational energy within each \mathcal{D} -dimensional class of $\text{SU}(2)$ -invariant PEPS i.e finding the optimum linear superposition of the \mathcal{D} independent tensors of each class. Since the number of variational parameters remains small (maximum of $\mathcal{D} = 30$ for $D = 7$) we have

used a “brute force” CG optimization as e.g. given in Numerical Recipes [76]. However, this requires an efficient iPEPS computation of the variational energy for any set of variational parameters to “feed” the CG routine. This is performed constructing a self-consistent environment around an active 2×2 cluster (see Fig. 2(b)) using an iterative CTM TRG algorithm [45–47] optimized for spatially symmetric tensors. Indeed, we have introduced simple modifications: (i) we use a *unique* CTM C tensor (side tensor T) which is the same for all corners (edges) and (ii) the basic Singular Value Decomposition (SVD) in each TRG step to construct the environment is replaced by a (more stable) ED, the CTM being here a symmetric matrix. The largest environment dimension we could handle was $\chi = 400$ and $\chi = 294$ for $D = 5$ and $D = 7$, respectively, for which up to 350 or 400 iterations became necessary to converge the environment. Note that the initial C (T) tensor is obtained from the \mathbb{I} tensor of Fig. 2(b) by summing over all external l and u (u) indices.

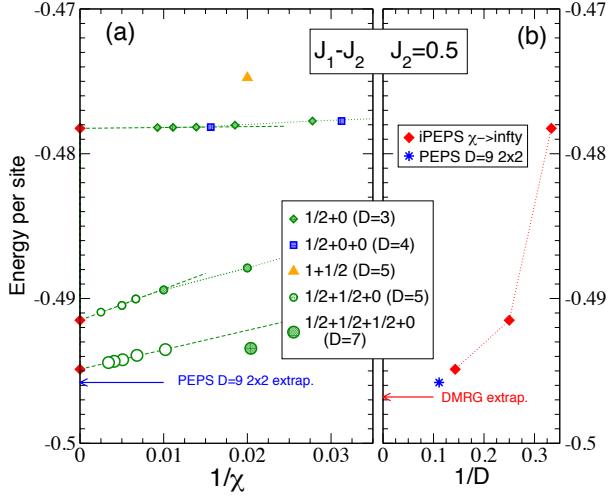


FIG. 3. [Color online] (a) iPEPS variational energies of the $J_1 - J_2$ model at $J_2 = 0.5$, versus the inverse of the environment dimension χ . Full (open) symbols correspond to fully optimized (fixed) tensor ansätze (see text). $\chi \rightarrow \infty$ linear extrapolations are performed using only the last data points. (b) Behavior of the $\chi \rightarrow \infty$ extrapolated energies vs the inverse of the bond dimension D . $D = 9$ PEPS [53] and DMRG [63] extrapolated energies are shown for comparison (see also Table I).

Energetics – Variational energies (per site) in each class of tensors are shown in Fig. 3(a) for $J_2 = 0.5$, as a function of the inverse of the environment dimension χ . A rapid comparison between the different classes (for intermediate χ) reveals that, for identical bond dimension D , the classes $V = \frac{1}{2}^{\otimes N} \oplus 0$ with $N = 1, 2$ and 3 (of bond dimensions $D = 3, 5$ and 7 , respectively) give the best results. Hence, hereafter we shall focus on this PEPS family defined in terms of N “colors” of spin- $\frac{1}{2}$. Note that the case $N = 1$ was studied previously in Ref. [66]. Tensors are fully optimized up to a maximum bond dimension χ_{opt} , e.g. for $D = 5$, $\chi_{\text{opt}} = 4D^2 = 100$ and, for $D = 7$, $\chi_{\text{opt}} = D^2 = 49$. Then, using environment dimensions $\chi > \chi_{\text{opt}}$ together with the fixed optimized tensor obtained at $\chi = \chi_{\text{opt}}$, one gets true *upper bounds* of the variational energy. In contrast, for $D = 3$, $\chi_{\text{opt}} = 12D^2 = 108$ already gives the absolute best tensor with enough accuracy. Generically, we found that the energy always decreases with increasing χ and, at large enough χ , linear fits can be performed in $1/\chi$ to provide $\chi \rightarrow \infty$ extrapolations, also upper bounds of the (D -dependent) variational energies. Note that our $D = 7$ extrapolation -0.49489 lies within only 0.2% of the extrapolated value -0.4958 obtained using cluster update finite size $D = 9$ PEPS [53]. We have plotted our ($\chi \rightarrow \infty$) results as a function of $1/D$ in Fig. 3(b) showing perfect consistency with the above-mentioned $D = 9$ result together with the DMRG extrapolation -0.4968 of Ref. 63. This agreement is remarkable considering the fact that we

use only a unique tensor parametrized by a small number of coefficients. Good variational energies have also been found for the simple NN Heisenberg model ($J_2 = 0$) as well as for larger frustration $J_2 = 0.55$ as shown in Appendix A. Our results are summarized in Table I and compared to the best estimates, from Quantum Monte Carlo at $J_2 = 0$ [5, 6] and from DMRG [63], VMC [67] and finite-size PEPS [53] at $J_2 = 0.5$ and $J_2 = 0.55$. We note however that our variational energies for $J_2 = 0$ and $J_2 = 0.55$ are slightly less accurate as for $J_2 = 0.5$. In fact, we believe J_{2c} is close to 0.5 and we argue below that our (optimized) PEPS is capable of picking up the critical nature of the QCP. For $J_2 = 0.55$ translation symmetry breaking is likely to occur spontaneously, which is not captured by our homogeneous ansatz. The ansatz does not either sustain magnetic LR order, that may explain its lower accuracy at $J_2 = 0$.

J	0	0.5	0.55
QMC	-0.66944		
DMRG		-0.4968	-0.4863
VMC		-0.4970(5)	-0.4870(5)
$D = 9$ PEPS		-0.4958(3)	-0.4857(2)
$D = 7$ iPEPS	-0.6677	-0.4949	-0.4830

TABLE I. Comparison between our $D = 7$ iPEPS results ($\chi \rightarrow \infty$ extrapolations) and the best estimates in the literature, for $J_2 = 0$, $J_2 = 0.5$ and $J_2 = 0.55$: $J_2 = 0$ results are obtained by QMC [5, 6]. At finite J_2 , we quote energies obtained by extrapolations to the thermodynamic limit using DMRG [63], VMC [67] and *finite-size* $D = 9$ PEPS [53]. Note that the $D = 7$ iPEPS energies are only upper bounds of the true variational energies (see text).

III. CORRELATION FUNCTIONS

Once the PEPS $|\Psi_0\rangle = |\Psi(D, \chi_{\text{opt}})\rangle$ has been optimized using the largest possible environment dimension $\chi = \chi_{\text{opt}}(D)$, various correlation functions can be computed (e.g. along the \mathbf{e}_x horizontal direction), like (i) the spin-spin correlations,

$$C_s(d) = \langle \mathbf{S}_i \cdot \mathbf{S}_{i+d\mathbf{e}_x} \rangle_0, \quad (1)$$

(ii) the (connected) *longitudinal* dimer-dimer correlations,

$$C_d^{(L)}(d) = \langle D_i^x D_{i+d\mathbf{e}_x}^x \rangle_0 - \langle D_i^x \rangle_0 \langle D_{i+d\mathbf{e}_x}^x \rangle_0, \quad (2)$$

and (iii) the (connected) *transverse* dimer-dimer correlations,

$$C_d^{(T)}(d) = \langle D_i^y D_{i+d\mathbf{e}_x}^y \rangle_0 - \langle D_i^y \rangle_0 \langle D_{i+d\mathbf{e}_x}^y \rangle_0, \quad (3)$$

where dimer operators $D_i^x = \mathbf{S}_i \cdot \mathbf{S}_{i+\mathbf{e}_x}$ and $D_i^y = \mathbf{S}_i \cdot \mathbf{S}_{i+\mathbf{e}_y}$ are oriented either along the \mathbf{e}_x (horizontal) or \mathbf{e}_y (vertical) directions, respectively, and the expectation values are taken in the optimized $|\Psi_0\rangle$ PEPS.

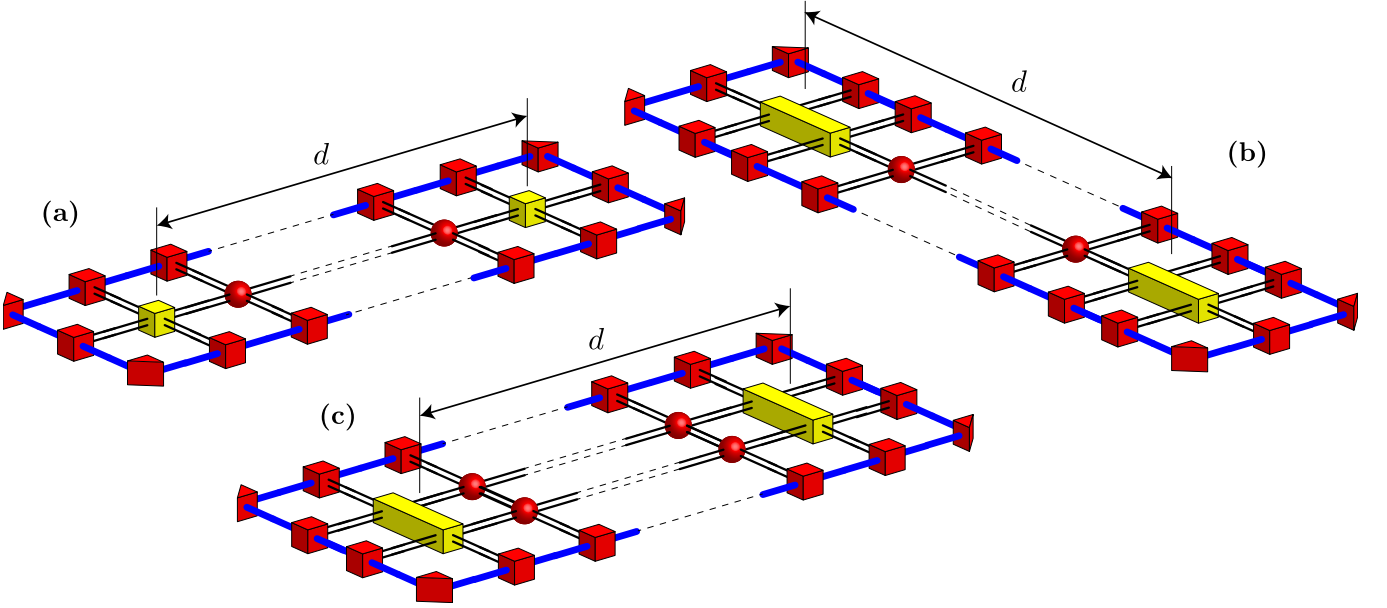


FIG. 4. [Color online] One dimensional strips used to compute the spin-spin (a), the longitudinal dimer-dimer (b) and the transverse dimer-dimer (c) correlation functions. A transfer matrix is applied recursively $d - 1$ times (a,c) or $d - 2$ times (b) in the direction of the strip.

The calculations of correlators are accomplished using the set-up shown in Fig. 4(a-c). Appropriate transfer matrices are used so that one can construct arbitrarily long strips. Here the site tensor is fixed to its optimized output (using $\chi = \chi_{\text{opt}}(D)$) while the environment dimension $\chi > \chi_{\text{opt}}(D)$ can be then further increased to reach convergence, which is easily achieved for short distance r . A comparison between the results obtained with the two ansätze $V = \frac{1}{2} \oplus \frac{1}{2} \oplus 0$ (a) and $V = \frac{1}{2} \oplus \frac{1}{2} \oplus \frac{1}{2} \oplus 0$ (b) is shown in Fig. 5 for $J_2 = 0.5$. Although a fast decay of the dimer-dimer correlations is seen in both cases, the behavior of the (staggered) spin-spin correlations is qualitatively different : for $D = 7$ $|C_s(r)|$ seems to approach a finite value while, for $D = 5$ (or $D = 3$ as well), it steadily decays to zero. This signals the emergence, for $D \geq 7$, of a finite staggered magnetization as defined by $m_{\text{stag}}(\chi) = \sqrt{\lim_{r \rightarrow \infty} |C_s(r)|}$. We note however that, strictly speaking, for finite χ the above limit should vanish since the correlations are cut-off above some correlation length $\xi_s(\chi)$ (see below). In other words, the strip of Fig. 4(a) is, crudely speaking, similar to a quasi-1D physical strip (ladder) of effective width $L_{\text{eff}}(\chi)$ [77], which, indeed, can not sustain long-range magnetic order from Mermin-Wagner theorem [78]. In practice, this argument does not apply since the SU(2) symmetry is not strictly enforced due to (i) the choice of the initial (CTM) conditions and (ii) the truncation procedure which does not preserve exactly the SU(2) multiplet structure. Small deviations from a perfectly SU(2)-symmetric environment act as a small symmetry-breaking (AF) "field" and the local spin operator acquires a finite value $\langle \mathbf{S}_i \rangle_0 = \cos(\mathbf{q}_{\text{AF}} \cdot \mathbf{i}) \mathbf{m}_{\text{stag}}$ oscillat-

ing at the antiferromagnetic wave vector \mathbf{q}_{AF} . As shown in Appendix B, $m_{\text{stag}}(\chi)$ vanishes in the $\chi \rightarrow \infty$ limit, physically corresponding to the limit of an infinitely wide strip $L_{\text{eff}} \rightarrow \infty$. This implies that the infinite 2D system recovers the full SU(2) spin symmetry encoded in the tensor ansatz. We have seen similar behaviors also for $J_2 = 0$ and $J_2 = 0.55$ as well (see Appendix B). Interestingly, the scaling of m_{stag} to zero may depend slightly of the initial CTM of the TRG procedure to converge the environment. In contrast, for $D = 3$ and $D = 5$ the system remains spin isotropic even for finite χ , the spin correlators $\langle S_i^\alpha S_j^\alpha \rangle_0$ being independent on $\alpha = x, y, z$, as checked explicitly. This signals a qualitative change of behavior when $N \geq 3$ which we identify in the next section.

Diverging correlation lengths – The results described above give some hints that, when $D = 7$, the spin-spin correlations become algebraic at long distance. However, for finite bond dimension χ , the strips of Fig. 4(a-c) can be seen as effective 1D systems. Then, finite correlation lengths $\xi_D(\chi)$ naturally emerge as the inverse of the gaps of *finite-dimensional* $D_{\text{eff}}^2 \times D_{\text{eff}}^2$ transfer matrices, where $D_{\text{eff}} = D\chi$ (Fig. 4(a,b)) or $D_{\text{eff}} = D^2\chi$ (Fig. 4(c)) are the effective dimensions of the associated 1D MPS. Using empirical findings for the correlation length ξ_{1D} in critical 1D systems [70–72], $\xi_{1D}(D) \sim D^\kappa$, one then expects that $\xi_D(\chi) \sim (D_{\text{eff}})^\kappa$, $\kappa > 0$, which should diverge with χ as a power law for critical PEPS. Hence, criticality (if any) is restored only in the $\chi \rightarrow \infty$ limit and finite- χ scaling is necessary to obtain informations on the QCP. Note that, when spin rotational symmetry is (artificially) broken at finite χ , it is important to consider the

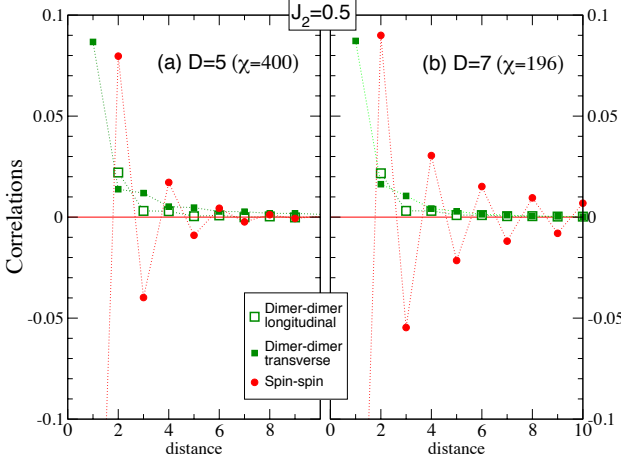


FIG. 5. [Color online] Short-distance correlation functions at $J_2 = 0.5$ for $V = \frac{1}{2} \oplus \frac{1}{2} \oplus 0$ (a) and $V = \frac{1}{2} \oplus \frac{1}{2} \oplus \frac{1}{2} \oplus 0$ (b). Large environment dimensions χ are used ensuring full convergence of the correlations at short distance ($r < 10$).

connected spin-spin correlator $\tilde{C}_s(d) = C_s(d) - (m_{\text{stag}})^2$. From straightforward fits of the long-distance correlations at $J_2 = 0.5$ (see Appendix C) we have extracted the correlation lengths $\xi_D(\chi)$ associated to the \tilde{C}_s , $C_d^{(T)}$ and $C_d^{(L)}$ correlation functions and results are shown in Fig. 6. For $D = 3$ or $D = 5$ we find a clear saturation of the spin-spin correlation lengths to small values while the dimer-dimer correlations lengths diverge *linearly* with χ . Such a behavior is typical of bi-partite dimer models [79] or of the NN RVB state on the square lattice [18, 19]. In fact, the $D = 3$ PEPS can be viewed as an extended-range RVB state [66] and the $D = 5$ PEPS as an extended-range *two-color* RVB state. Plotting the dimer correlation lengths in Fig. 6(c,e) as a function of χ/D^2 clearly reveals the similarities between $D = 5$ and $D = 7$. However, in the case of the spin correlations, a sudden qualitative change occurs at $D = 7$ for which we find that the spin-spin correlation length no longer saturates but diverges linearly with χ , as the dimer correlation lengths do. This suggests that the (optimized) $D = 7$ PEPS is fully critical in the limit $\chi \rightarrow \infty$.

Power-law exponents – Whenever the correlation length $\xi_D(\chi)$ diverges, one might expect to see power-law behaviors in the correlation functions,

$$C_s(d) \sim d^{-(1+\eta_s)}, \quad (4)$$

$$C_d(d) \sim d^{-(1+\eta_d)}, \quad (5)$$

in the range of distance $1 < d < \xi_D$, where η_s and η_d defined e.g. in Ref. [80] are the anomalous dimensions. Note however that this scaling regime can be observed only when $\xi_D(\chi)$ has reached a sufficiently large value. To obtain estimates of the exponents $1 + \eta_s$ and $1 + \eta_d$ we have plotted spin-spin and (transverse) dimer-dimer

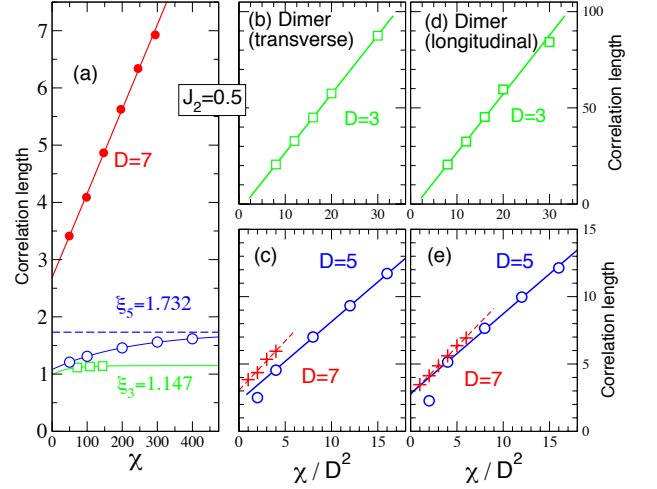


FIG. 6. [Color online]) Scaling of the various correlation lengths at $J_2 = 0.5$ vs environment dimension χ (left panel) or χ/D^2 (right panels), for $V = \frac{1}{2} \oplus 0$ (open squares), $V = \frac{1}{2} \oplus \frac{1}{2} \oplus 0$ (open circles) and $V = \frac{1}{2} \oplus \frac{1}{2} \oplus \frac{1}{2} \oplus 0$ (large dots and crosses). (a) Spin-spin correlations; (b,c) Transverse dimer-dimer correlations; (d,e) Longitudinal dimer-dimer correlations.

correlations at $J_2 = 0.5$ in Fig. 7(a,b) using log-log scales. For $D = 3$ ($D = 5$) the dimer correlation length is very large (is large) for the largest χ we can reach and, from fits of the data in the range $1 < d < 100$ ($1 < d < 20$), one can easily extract the exponent $1 + \eta_d \simeq 1.25$ ($1 + \eta_d \simeq 1.5$). For $D = 7$, it is difficult to extract accurate exponents since cross-overs to exponential decays occur rapidly around $d \sim \xi_7 \simeq 6$, for both the spin-spin and dimer-dimer correlations. However, the systematic trend of the data with χ in Fig. 7(a) suggests $\eta_s < 0.6$. In addition, we observe strong similarities between the linear scalings of the dimer correlation lengths for $D = 5$ and $D = 7$ once plotted vs χ/D^2 as shown in Fig. 7(d,e). This may indicate that the dimer anomalous dimension η_d for $D = 7$ is still close to its $D = 5$ estimate $\eta_d \sim 0.5$.

Discussion and outlook – We argue that the family of $SU(2)$ -symmetric tensors characterized by the virtual space $V = \frac{1}{2}^{\otimes N} \oplus 0$ and bond dimension $D = 2N + 1$ can describe faithfully the QCP of the spin- $\frac{1}{2}$ $J_1 - J_2$ Heisenberg model, provided the number of “colors” is large enough, i.e $N \geq 3$. For $N = 3$ ($D = 7$), we gave convincing evidence for a critical state exhibiting power law decaying spin-spin and dimer-dimer correlation functions. Related $J - Q$ models can be investigated with QMC [80] and $\eta_s \simeq 0.35(2)$ and $\eta_d \simeq 0.20(2)$ have been obtained (for the $J - Q_2$ model), which seem to deviate substantially from our findings $\eta_s < 0.6$ and $\eta_d \sim 0.5$ obtained at $N = 3$ ($D = 7$).

It is a general trend that spin-spin correlations decay less rapidly for increasing D so we expect such corre-

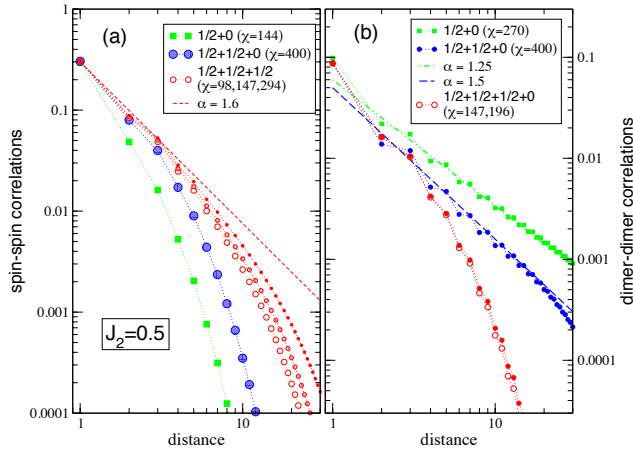


FIG. 7. [Color online] (a) Log-log plot of spin-spin (a) and transverse dimer-dimer (b) correlations versus distance. Straight (dashed) lines correspond to power-law decays $\sim d^{-\alpha}$.

lations to remain critical for $N > 3$. In addition, we observe that dimer-dimer correlations (and correlation lengths) are very similar for $N = 2$ and $N = 3$, if compared at the same value of the ratio χ/D^2 . In fact, we

may speculate that, for $N \geq 3$, all correlation lengths diverge as

$$\xi_D(\chi) \simeq f_D \chi/D^2, \quad (6)$$

where the prefactor f_D depends weakly on D , the main effect of increasing the bond dimension being to rescale the environment dimension $\chi \rightarrow \chi_D = \chi/D^2$. That would strongly suggest that η_s and η_d obtained in the limit $\chi_D \rightarrow \infty$ only weakly depend on D . For example, η_d might remain close, for $D \rightarrow \infty$, to the estimate $\eta_d \simeq 0.5$ extracted here for $D = 5$.

ACKNOWLEDGMENTS

This project is supported by the TNSTRONG ANR grant (French Research Council). This work was granted access to the HPC resources of CALMIP supercomputing center under the allocations 2016-P1231 and 2017-P1231. DP thanks Nicolas Renon (CALMIP) and Cyril Mazauric (ATOS) for assistance. DP acknowledges illuminating discussions with Philippe Corboz, as well as helpful advices to implement the CTM algorithm. MM and DP thank Roman Orus for insightful comments. DP also acknowledges inspiring conversations with Fabien Alet, Federico Becca, Ignacio Cirac, Shenghan Jiang, Naoki Kawashima, Frédéric Mila, David Perez-Garcia, Frank Pollmann, Pierre Pujol, Ying Ran, Anders Sandvik, Norbert Schuch, Frank Verstraete and Ling Wang.

-
- [1] Matthieu Mambrini, Román Orús, and Didier Poilblanc, “Systematic construction of spin liquids on the square lattice from tensor networks with SU(2) symmetry,” *Phys. Rev. B* **94**, 205124 (2016).
 - [2] T. Senthil, Ashvin Vishwanath, Leon Balents, Subir Sachdev, and Matthew P. A. Fisher, “Deconfined quantum critical points,” *Science* **303**, 1490–1494 (2004).
 - [3] Hui Shao, Wenan Guo, and Anders W. Sandvik, “Quantum criticality with two length scales,” *Science* **352**, 213–216 (2016).
 - [4] J. D. Reger and A. P. Young, “Monte carlo simulations of the spin-1/2 heisenberg antiferromagnet on a square lattice,” *Phys. Rev.* **37**, 5978 (1988).
 - [5] A. W. Sandvik and H. G. Evertz, “Loop updates for variational and projector quantum monte carlo simulations in the valence-bond basis,” *Phys. Rev.* **82**, 024407 (2010).
 - [6] A. W. Sandvik, “Computational studies of quantum spin systems,” in *XIV Training Course in the Physics of Strongly Correlated Systems, Salerno (Vietri sul Mare), Italy, October 5-16, 2009*, Vol. 1297, edited by Adolfo Avella and Ferdinando Mancini (American Institute of Physics, 2010) p. 135.
 - [7] P. Chandra and B. Douçot, “Possible spin-liquid state at large S for the frustrated square heisenberg lattice,” *Phys. Rev. B* **38**, 9335–9338 (1988).
 - [8] E. Dagotto and A. Moreo, “Exact diagonalization study of the frustrated heisenberg model: A new disordered phase,” *Phys. Rev. B* **39**, 4744–4747 (1989).
 - [9] Subir Sachdev and N. Read, “Large N expansion for frustrated and doped quantum antiferromagnets,” *International Journal of Modern Physics B* **05**, 219–249 (1991).
 - [10] F. Mila, D. Poilblanc, and C. Bruder, “Spin dynamics in a frustrated magnet with short-range order,” *Phys. Rev. B* **43**, 7891–7898 (1991).
 - [11] N. Read and Subir Sachdev, “Valence-bond and spin-peierls ground states of low-dimensional quantum antiferromagnets,” *Phys. Rev. Lett.* **62**, 1694–1697 (1989).
 - [12] Elbio Dagotto and Adriana Moreo, “Phase diagram of the frustrated spin-1/2 heisenberg antiferromagnet in 2 dimensions,” *Phys. Rev. Lett.* **63**, 2148–2151 (1989).
 - [13] Didier Poilblanc, Eduardo Gagliano, Silvia Bacci, and Elbio Dagotto, “Static and dynamical correlations in a spin-1/2 frustrated antiferromagnet,” *Phys. Rev. B* **43**, 10970–10983 (1991).
 - [14] H.J. Schulz, T.A.L. Ziman, and D. Poilblanc, “Magnetic order and disorder in the frustrated quantum heisenberg antiferromagnet in two dimensions,” *J. Phys. I France* **6**, 675–703 (1996).
 - [15] M. E. Zhitomirsky and Kazuo Ueda, “Valence-bond crystal phase of a frustrated spin-1/2 square-lattice antiferromagnet,” *Phys. Rev. B* **54**, 9007–9010 (1996).
 - [16] Matthieu Mambrini, Andreas Läuchli, Didier Poilblanc, and Frédéric Mila, “Plaquette valence-bond crystal in the frustrated heisenberg quantum antiferromagnet on the

- square lattice,” *Phys. Rev. B* **74**, 144422 (2006).
- [17] P.W. Anderson, “Resonating valence bonds: A new kind of insulator?” *Materials Research Bulletin* **8**, 153 – 160 (1973).
 - [18] A. Fabricio Albuquerque and Fabien Alet, “Critical correlations for short-range valence-bond wave functions on the square lattice,” *Phys. Rev. B* **82**, 180408 (2010).
 - [19] Didier Poilblanc, Norbert Schuch, David Pérez-García, and J. Ignacio Cirac, “Topological and entanglement properties of resonating valence bond wave functions,” *Phys. Rev. B* **86**, 014404 (2012).
 - [20] Norbert Schuch, Didier Poilblanc, J. Ignacio Cirac, and David Pérez-García, “Resonating valence bond states in the PEPS formalism,” *Physical Review B* **86**, 115108 (2012).
 - [21] J. Ignacio Cirac and Frank Verstraete, “Renormalization and tensor product states in spin chains and lattices,” *Journal of Physics A: Mathematical and Theoretical* **42**, 504004 (2009), [arXiv:0910.1130](#).
 - [22] J. I. Cirac, “Entanglement in many-body quantum systems,” in *Many-Body Physics with ultracold atoms* (Les Houches school, 2010).
 - [23] Román Orús, “A practical introduction to tensor networks: Matrix product states and projected entangled pair states,” *Annals of Physics* **349**, 117–158 (2014).
 - [24] Norbert Schuch, “Condensed matter applications of entanglement theory,” in *Quantum Information Processing: Lecture Notes*, Schriften des Forschungszentrums Jülich. Reihe Schlüsseltechnologien / Key Technologies, 44th IFF Spring School (David P. DiVincenzo, Forschungszentrum Jülich, 2013) p. 29.
 - [25] Román Orús, “Advances on tensor network theory: symmetries, fermions, entanglement, and holography,” *The European Physical Journal B* **87**, 1–18 (2014).
 - [26] S. R. White, “Density matrix formulation for quantum renormalization groups,” *Physical Review Letters* **69**, 2863–2866 (1992).
 - [27] David Pérez-García, Frank Verstraete, J. Ignacio Cirac, and Michael M. Wolf, “PEPS as unique ground states of local Hamiltonians,” *Quant. Inf. Comp.* **8**, 0650 (2008), [arXiv:0707.2260](#).
 - [28] David Pérez-García, M Sanz, C E González-Guillén, M M Wolf, and J. Ignacio Cirac, “Characterizing symmetries in a projected entangled pair state,” *New Journal of Physics* **12**, 025010 (2010).
 - [29] Norbert Schuch, J. Ignacio Cirac, and David Pérez-García, “PEPS as ground states: Degeneracy and topology,” *Annals of Physics* **325**, 2153–2192 (2010).
 - [30] Sukhwinder Singh, Robert N. C. Pfeifer, and Guifré Vidal, “Tensor network decompositions in the presence of a global symmetry,” *Phys. Rev. A* **82**, 050301 (2010).
 - [31] Sukhwinder Singh and Guifré Vidal, “Tensor network states and algorithms in the presence of a global $su(2)$ symmetry,” *Phys. Rev. B* **86**, 195114 (2012).
 - [32] Sukhwinder Singh and Guifré Vidal, “Global symmetries in tensor network states: Symmetric tensors versus minimal bond dimension,” *Phys. Rev. B* **88**, 115147 (2013).
 - [33] Andreas Weichselbaum, “Non-abelian symmetries in tensor networks: A quantum symmetry space approach,” *Annals of Physics* **327**, 2972 – 3047 (2012).
 - [34] Shenghan Jiang and Ying Ran, “Symmetric tensor networks and practical simulation algorithms to sharply identify classes of quantum phases distinguishable by short-range physics,” *Phys. Rev. B* **92**, 104414 (2015).
 - [35] Jutho Haegeman, Karel Van Acoleyen, Norbert Schuch, J. Ignacio Cirac, and Frank Verstraete, “Gauging quantum states: From global to local symmetries in many-body systems,” *Phys. Rev. X* **5**, 011024 (2015).
 - [36] J. Ignacio Cirac, Didier Poilblanc, Norbert Schuch, and Frank Verstraete, “Entanglement spectrum and boundary theories with projected entangled-pair states,” *Physical Review B* **83**, 245134 (2011).
 - [37] S. Yang, L. Lehman, D. Poilblanc, K. Van Acoleyen, F. Verstraete, J. I. Cirac, and N. Schuch, “Edge theories in projected entangled pair state models,” *Phys. Rev. Lett.* **112**, 036402 (2014).
 - [38] Chao-Ming Jian and Michael Zaletel, “Existence of featureless paramagnets on the square and the honeycomb lattices in 2+1 dimensions,” *Phys. Rev. B* **93**, 035114 (2016).
 - [39] Didier Poilblanc and Norbert Schuch, “Simplex \mathbb{Z}_2 spin liquids on the kagome lattice with projected entangled pair states: Spinon and vison coherence lengths, topological entropy, and gapless edge modes,” *Physical Review B* **87**, 140407 (2013).
 - [40] Wei Li, Shuo Yang, Meng Cheng, Zheng-Xin Liu, and Hong-Hao Tu, “Topology and criticality in the resonating afleck-kennedy-lieb-tasaki loop spin liquid states,” *Phys. Rev. B* **89**, 174411 (2014).
 - [41] Didier Poilblanc, Norbert Schuch, and J. Ignacio Cirac, “Field-induced superfluids and Bose liquids in projected entangled pair states,” *Physical Review B* **88**, 144414 (2013).
 - [42] Didier Poilblanc, Philippe Corboz, Norbert Schuch, and J. Ignacio Cirac, “Resonating-valence-bond superconductors with fermionic projected entangled pair states,” *Physical Review B* **89**, 241106 (2014).
 - [43] Jutho Haegeman and Frank Verstraete, “Diagonalizing transfer matrices and matrix product operators: a medley of exact and computational methods,” *Lecture Notes, Vienna University*, [arXiv:1611.08519](#).
 - [44] J. Jordan, R. Orús, G. Vidal, Verstraete F., and J.I. Cirac, “xxx,” *Phys. Rev. Letters* **101**, 250602 (2008).
 - [45] Tomotoshi Nishino and Kouichi Okunishi, “Corner transfer matrix renormalization group method,” *Journal of the Physical Society of Japan* **65**, 891–894 (1996), <http://dx.doi.org/10.1143/JPSJ.65.891>.
 - [46] Román Orús and Guifré Vidal, “Simulation of two-dimensional quantum systems on an infinite lattice revisited: Corner transfer matrix for tensor contraction,” *Physical Review B* **80**, 094403 (2009).
 - [47] Román Orús, “Exploring corner transfer matrices and corner tensors for the classical simulation of quantum lattice systems,” *Physical Review B* **85**, 205117 (2012).
 - [48] G. Vidal, “Classical Simulation of Infinite-Size Quantum Lattice Systems in One Spatial Dimension,” *Physical Review Letters* **98**, 5 (2007).
 - [49] Román Orús and G. Vidal, “Infinite time-evolving block decimation algorithm beyond unitary evolution,” *Physical Review B* **78**, 155117 (2008).
 - [50] G. Vidal, “Efficient Classical Simulation of Slightly Entangled Quantum Computations,” *Physical Review Letters* **91**, 4 (2003), [arXiv:0301063 \[quant-ph\]](#).
 - [51] H. C. Jiang, Z. Y. Weng, and T. Xiang, “Accurate determination of tensor network state of quantum lattice models in two dimensions,” *Phys. Rev. Lett.* **101**, 090603 (2008).
 - [52] Ho N. Phien, Johann A. Bengua, Hoang D. Tuan,

- Philippe Corboz, and Román Orús, “Infinite projected entangled pair states algorithm improved: Fast full update and gauge fixing,” *Phys. Rev. B* **92**, 035142 (2015).
- [53] Ling Wang, Zheng-Cheng Gu, Frank Verstraete, and Xiao-Gang Wen, “Tensor-product state approach to spin- $\frac{1}{2}$ square J_1 – J_2 antiferromagnetic heisenberg model: Evidence for deconfined quantum criticality,” *Phys. Rev. B* **94**, 075143 (2016).
- [54] Philippe Corboz, “Variational optimization with infinite projected entangled-pair states,” *Phys. Rev. B* **94**, 035133 (2016).
- [55] Laurens Vanderstraeten, Jutho Haegeman, Philippe Corboz, and Frank Verstraete, “Gradient methods for variational optimization of projected entangled-pair states,” *Phys. Rev. B* **94**, 155123 (2016).
- [56] Wen-Yuan Liu, Shao-Jun Dong, Yong-Jian Han, Guang-Can Guo, and Lixin He, “Gradient optimization of finite projected entangled pair states,” [arXiv:1611.09467](https://arxiv.org/abs/1611.09467).
- [57] Ann B. Kallin, Matthew B. Hastings, Roger G. Melko, and Rajiv R. P. Singh, “Anomalies in the entanglement properties of the square-lattice heisenberg model,” *Phys. Rev. B* **84**, 165134 (2011).
- [58] M. A. Metlitski and T. Grover, “Entanglement entropy of systems with spontaneously broken continuous symmetry,” (2011), [http://arxiv.org/abs/1112.5166](https://arxiv.org/abs/1112.5166).
- [59] Hyejin Ju, Ann B. Kallin, Paul Fendley, Matthew B. Hastings, and Roger G. Melko, “Entanglement scaling in two-dimensional gapless systems,” *Phys. Rev. B* **85**, 165121 (2012).
- [60] Didier Poilblanc, “Entanglement hamiltonian of the quantum nelson state,” *Journal of Statistical Mechanics: Theory and Experiment* **2014**, P10026 (2014).
- [61] Michael Lubasch, J. Ignacio Cirac, and Mari-Carmen Bañuls, “Algorithms for finite projected entangled pair states,” *Phys. Rev. B* **90**, 064425 (2014).
- [62] Luca Capriotti and Sandro Sorella, “Spontaneous plaquette dimerization in the J_1 – J_2 heisenberg model,” *Phys. Rev. Lett.* **84**, 3173–3176 (2000).
- [63] Shou-Shu Gong, Wei Zhu, D. N. Sheng, Olexei I. Motrunich, and Matthew P. A. Fisher, “Plaquette ordered phase and quantum phase diagram in the spin- $\frac{1}{2}$ J_1 – J_2 square heisenberg model,” *Phys. Rev. Lett.* **113**, 027201 (2014).
- [64] Hong-Chen Jiang, Hong Yao, and Leon Balents, “Spin liquid ground state of the spin- $\frac{1}{2}$ square J_1 – J_2 heisenberg model,” *Phys. Rev. B* **86**, 024424 (2012).
- [65] Luca Capriotti, Federico Becca, Alberto Parola, and Sandro Sorella, “Resonating valence bond wave functions for strongly frustrated spin systems,” *Phys. Rev. Lett.* **87**, 097201 (2001).
- [66] Ling Wang, Didier Poilblanc, Zheng-Cheng Gu, Xiao-Gang Wen, and Frank Verstraete, “Constructing a Gapless Spin-Liquid State for the Spin-1/2 J_1 – J_2 Heisenberg Model on a Square Lattice,” *Physical Review Letters* **111**, 037202 (2013).
- [67] Wen-Jun Hu, Federico Becca, Alberto Parola, and Sandro Sorella, “Direct evidence for a gapless Z_2 spin liquid by frustrating Néel antiferromagnetism,” *Phys. Rev. B* **88**, 060402 (2013).
- [68] Ling Wang and Anders Sandvik, “unpublished,” (2017).
- [69] Ryui Kaneko, Luca F. Tocchio, Roser Valentí, Federico Becca, and Claudius Gros, “Spontaneous symmetry breaking in correlated wave functions,” *Phys. Rev. B* **93**, 125127 (2016).
- [70] L. Tagliacozzo, Thiago. R. de Oliveira, S. Iblisdir, and J. I. Latorre, “Scaling of entanglement support for matrix product states,” *Phys. Rev. B* **78**, 024410 (2008).
- [71] Frank Pollmann, Subroto Mukerjee, Ari M. Turner, and Joel E. Moore, “Theory of finite-entanglement scaling at one-dimensional quantum critical points,” *Phys. Rev. Lett.* **102**, 255701 (2009).
- [72] B. Pirvu, G. Vidal, F. Verstraete, and L. Tagliacozzo, “Matrix product states for critical spin chains: Finite-size versus finite-entanglement scaling,” *Phys. Rev. B* **86**, 075117 (2012).
- [73] Chen Liu, Ling Wang, Anders W. Sandvik, Yu-Cheng Su, and Ying-Jer Kao, “Symmetry breaking and criticality in tensor-product states,” *Phys. Rev. B* **82**, 060410 (2010).
- [74] F. Verstraete, M. Wolf, David Pérez-García, and J. I. Cirac, “Criticality, the Area Law, and the Computational Power of Projected Entangled Pair States,” *Physical Review Letters* **96**, 220601 (2006).
- [75] Didier Poilblanc and Matthieu Mambrini, “Supplemental material : Classification of all SU(2)-invariant S=1/2 D=7 tensors and expressions of all 30 A_1 D=7 tensors (zip file).” .
- [76] William H. Press, Saul A. Teukolsky, William P. Vetterling, and Brian P. Flannery, *Numerical Recipes* (Cambridge University Press, 2007).
- [77] T. Nishino, K. Okunishi, and M. Kikuchi, “Numerical renormalization group at criticality,” *Physics Letters A* **213**, 69 – 72 (1996).
- [78] N. D. Mermin and H. Wagner, “Absence of ferromagnetism or antiferromagnetism in one- or two-dimensional isotropic heisenberg models,” *Phys. Rev. Lett.* **17**, 1133–1136 (1966).
- [79] Anders W. Sandvik and R. Moessner, “Correlations and confinement in nonplanar two-dimensional dimer models,” *Phys. Rev. B* **73**, 144504 (2006).
- [80] Jie Lou, Anders W. Sandvik, and Naoki Kawashima, “Antiferromagnetic to valence-bond-solid transitions in two-dimensional SU(N) heisenberg models with multi-spin interactions,” *Phys. Rev. B* **80**, 180414 (2009).

Appendix A: Scaling of the $D = 7$ variational energy vs inverse environment dimension

We report in Fig. 8(a-c) the variational energies of the $V = \frac{1}{2} \oplus \frac{1}{2} \oplus \frac{1}{2} \oplus 0$ PEPS ansatz for the $J_1 - J_2$ model at $J_2 = 0$ (unfrustrated case), $J_2 = 0.5$ and $J_2 = 0.55$. The parameters of the PEPS are optimized with an environment dimension $\chi_{\text{opt}} = D^2 = 49$, independently for each value of J_2 . The environment dimension $\chi > \chi_{\text{opt}}$ is then increased, keeping the PEPS tensor fixed, and the energy is extrapolated linearly with $1/\chi$. At $J_2 = 0.5$, an excellent agreement is found with extrapolation from $D = 9$ PEPS cluster update [53]. For $J_2 = 0$ and $J_2 = 0.55$ a less good agreement is found with QMC [5, 6] and $D = 9$ PEPS cluster update [53], respectively (see text for explanation).

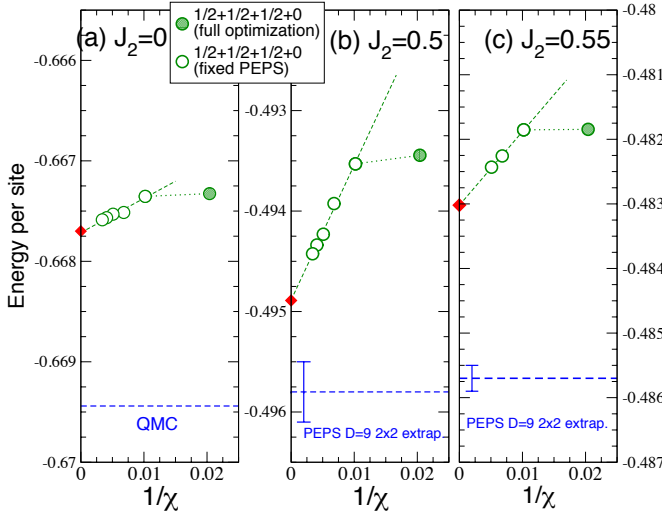


FIG. 8. [Color online] (a) $D = 7$ iPEPS variational energies of the $J_1 - J_2$ model at $J_2 = 0$ (a), $J_2 = 0.5$ (b) and $J_2 = 0.55$, versus the inverse of the environment dimension χ . Full (open) symbols correspond to fully optimized (fixed) tensor ansätze (see text). $\chi \rightarrow \infty$ linear extrapolations are performed using only the last data points. Comparisons with QMC [5, 6] and *finite size* $D = 9$ PEPS extrapolations (with error bars) [53] are shown.

Appendix B: Scaling of the $D = 7$ staggered magnetization vs inverse environment dimension

We report in Fig. 9(a-c) the spurious staggered magnetization of the $V = \frac{1}{2} \oplus \frac{1}{2} \oplus \frac{1}{2} \oplus 0$ PEPS ansatz for the $J_1 - J_2$ model at $J_2 = 0$ (unfrustrated case), $J_2 = 0.5$ and $J_2 = 0.55$. The procedure is the same as in Appendix A and the data are plotted vs χ . For all J_2 values, the scaling (algebraic fits) is consistent with vanishing m_{stag} when $\chi \rightarrow \infty$. Full $SU(2)$ invariance is recovered in this case.

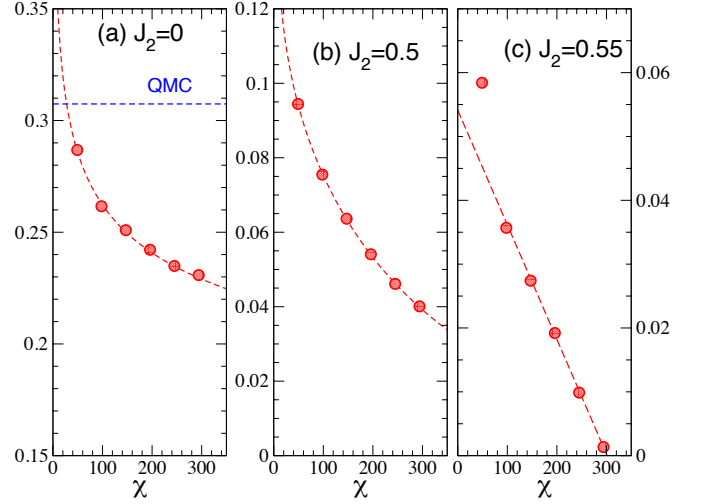


FIG. 9. [Color online] (a) $D = 7$ iPEPS staggered magnetization of the $J_1 - J_2$ model at $J_2 = 0$ (a), $J_2 = 0.5$ (b) and $J_2 = 0.55$, versus environment dimension χ . $\chi \rightarrow \infty$ extrapolations are based on power-law fits. The exact (QMC) value of m_{stag} [5, 6] at $J_2 = 0$ is shown.

Appendix C: Extracting the correlation lengths $\xi_D(\chi)$ from the long distance correlations

In order to extract the correlation lengths associated to the various correlation functions $C_\lambda(d)$ ($\lambda = S, D$) defined in the paper in Eqs. (1), (2) and (3), we have computed the long-distance correlations using the transfer matrix methods sketched in Fig. 2. Due to a finite gap in the relevant transfer matrices for all finite dimensions D and χ , one expects an exponential decay of all correlations,

$$C_\lambda(d) \sim C_0 \exp(-d/\xi_D(\chi)),$$

at sufficiently large distance d (typically $d > \xi_D(\chi)$). Let us summarize the procedure : First, the local tensors for $D = 3, 5$ and 7 are obtained by a full CG optimization (for $J_2 = 0.5$) using a given environment dimension $\chi_{\text{opt}} = 108, 100$ and 49 , respectively. The correlations in these fixed PEPS are then computed for increasing values of the environment dimension χ in two steps : (i) For every choice of $\chi \geq \chi_{\text{opt}}$, the new converged CTM C and edge tensor T are computed (by the iterative renormalization scheme) and, finally, (ii) used to compute the correlation functions in the setup shown in Fig. 2(a-c). Results are displayed using semi-logarithmic scales in Figs. 10(a), 11(a) and 12(a). By fitting the asymptotic linear behaviors of the data according to $\ln C_\lambda(d) = -(1/\xi)d + c_0$, one straightforwardly gets the correlation lengths ξ from the slopes $-1/\xi$.

The scaling of the correlation lengths ξ_D with χ are shown in Figs. 10(b), 11(b,c) and 12(b,c). For $D = 3$ and $D = 5$, one observes a clear saturation of the spin correlation lengths ξ_3 and ξ_5 to rather small values (less

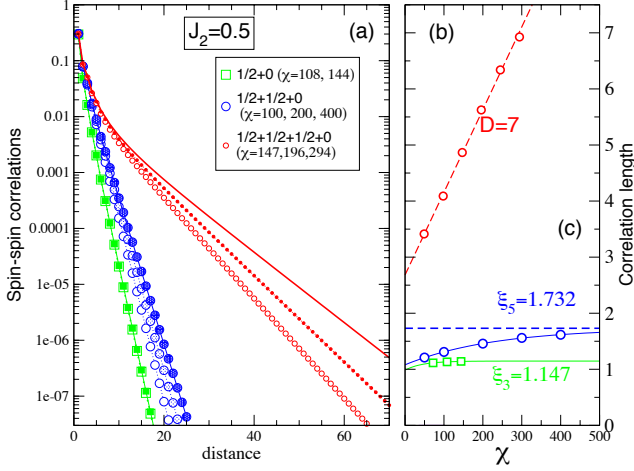


FIG. 10. [Color online] (a) Spin-spin correlation versus distance for (fixed) $D = 3$, $D = 5$ and $D = 7$ tensors and several dimension χ of the environment (semi-log scale). The tensors are obtained from a full CG optimization using environment dimensions $\chi_{\text{opt}} = 108, 100$ and 49 , respectively. Correlation length extracted from linear fits of the asymptotic large-distance behaviors are shown in (b) versus χ .

than 2 lattice spacings) while the dimer correlation length scales linearly with χ suggesting that $\xi_D \rightarrow \infty$ in the limit $\chi \rightarrow \infty$, for which the calculation becomes exact. Note that the (extrapolated) spin correlation length increases with D while the divergence of the dimer correlation length becomes weaker. For $D = 7$, one has to consider the *connected* part of the spin-spin correlation, subtracting off the contribution from the spurious staggered spin density background. The spin correlation length no longer saturates but rather increases linearly with the environment dimension χ . This strongly suggests that ξ_7 diverges in the limit $\chi \rightarrow \infty$, that is consistent with a power-law decay of the correlation function. We believe our data also support the divergence of the dimer correlation length as well.

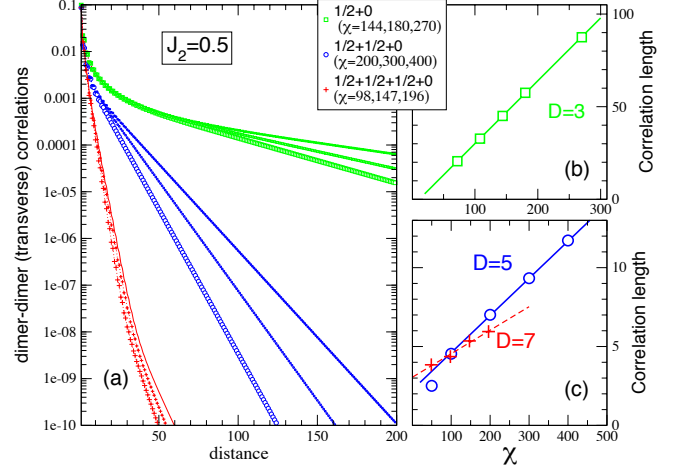


FIG. 11. [Color online] (a) Transverse dimer-dimer correlation versus distance for $D = 3$, $D = 5$ and $D = 7$ tensors and several values of χ (semi-log scale). Tensors are the same as in Fig. 10. Correlation lengths extracted from linear fits of the asymptotic large-distance behaviors are shown in (b) and (c) versus χ .

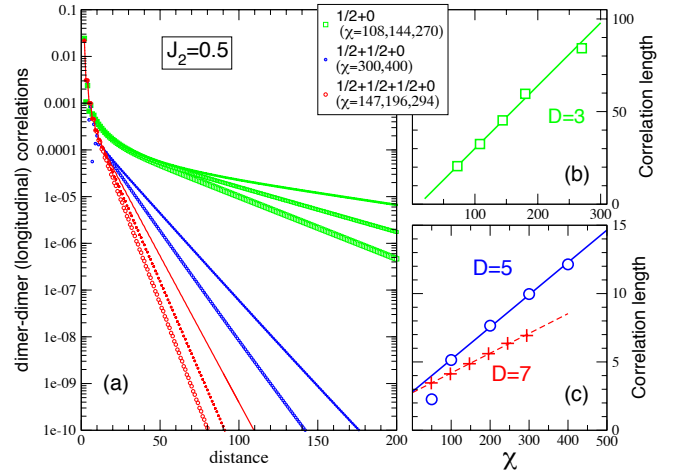


FIG. 12. [Color online] (a) Longitudinal dimer-dimer correlation versus distance for $D = 3$, $D = 5$ and $D = 7$ tensors and several values of χ (semi-log scale). Tensors are the same as in Fig. 10. Correlation lengths extracted from linear fits of the asymptotic large-distance behaviors are shown in (b) and (c) versus χ .